UCRL-JC-105847
PREPRINT

Real-Time Wavefront Correction System Using a Zonal Deformable Mirror and a Hartmann Sensor

J. Thaddeus Salmon, Erlan S. Bliss,
Theresa W. Long, Edward L. Orham,
Robert W. Presta, Charles D. Swift,
Richard S. Ward

This Paper Was Prepared For Submittal To
SPIE's International Symposium on
Optical Applied Science and Engineering
San Diego, CA
July 21-26, 1991

July 1991

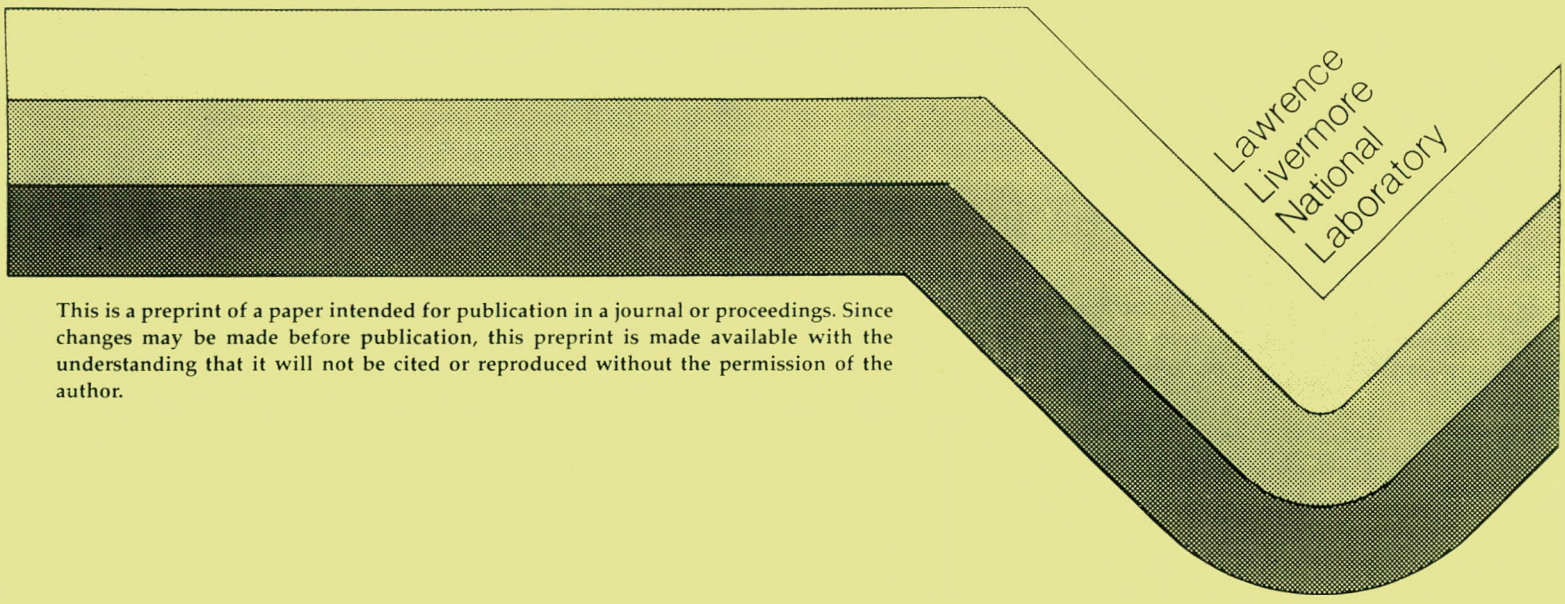

UCRL-JC--105847

DE92 006891

Real-time wavefront correction system using a zonal deformable mirror and a Hartmann sensor*

J. Thaddeus Salmon, Erlan S. Bliss, Theresa W. Long, Edward L. Orham,
Robert W. Presta, Charles D. Swift, Richard S. Ward

Lawrence Livermore National Laboratory
P.O. Box 808, MS L-463
Livermore, CA 94550

ABSTRACT

We have developed an adaptive optics system that corrects up to five waves of 2nd-order and 3rd-order aberrations in a high-power laser beam to less than 1/10th wave RMS. The wavefront sensor is a Hartmann sensor with discrete lenses and position-sensitive photodiodes; the deformable mirror uses piezoelectric actuators with feedback from strain gauges bonded to the stacks. The controller hardware uses a VME bus. The system removes thermally induced aberrations generated in the master-oscillator-power-amplifier chains of a dye laser, as well as aberrations generated in beam combiners and vacuum isolation windows for average output powers exceeding 1 kW. The system bandwidth is 1 Hz, but higher bandwidths are easily attainable.

1. INTRODUCTION

Atomic Vapor Laser Isotope Separation requires the copropagation of multiple beams at different wavelengths and at average powers exceeding 1 kW.[1] Although we use mirror coatings that absorb less than one part in 10^5, the beams still suffer from thermally induced phase distortions, both in the dye amplifiers and in transmissive optics, such as beam combiners and vacuum windows. These aberrations are 2nd-order and 3rd-order and can reach 5 waves peak-to-valley (p-v), which causes the beam to distort and break up when propagated over large distances. The magnitude of the aberrations scales with power, with time constants on the order of 30 seconds.

We have developed an adaptive optics system that corrects thermally induced phase distortions of both 2nd-order and 3rd-order. The closed-loop bandwidth of the system is about 1 Hz, which is much less than the observed time constants associated with these aberrations. This paper will describe (1) the components of the system, (2) the algorithm used by the controller, and (3) the testing of system performance in the laboratory.

2. SYSTEM DESCRIPTION

The adaptive optics system consists of a wavefront sensor, a deformable mirror, and controller hardware and software. A schematic of the system is shown in Fig. 1. Overall tilt is controlled by an independent alignment control system. An interferometer, calibrated to a wavefront reference source, continually monitors the wavefront after the deformable mirror and documents system performance. The interferometer also diagnoses the reflected wavefront during open-loop flattening of the mirror, which is accomplished before calibrating the system. All adaptive optics systems are accessible via Ethernet from workstations in the area. The following sections will describe the wavefront sensor, the deformable mirror, and the controller hardware and software.

---

*Work performed under the auspices of the U.S. Department of Energy by the Lawrence Livermore National Laboratory under Contract W-7405-Eng-48.

2.1 Wavefront Sensor

The wavefront sensor is a discrete Hartmann-Shack design[2], which is shown schematically in Fig. 2. The sensor uses a 4x8 array of discrete lenses, each of which samples a part of the laser beam and focuses light onto a lateral field-effect photodiode. The local x- and y-components of the angular tilt in the wavefront, averaged over the aperture of each lenslet, are given by the partial derivatives

$$\frac{\partial \phi}{\partial x} = f (x - x_0) \tag{1}$$

and

$$\frac{\partial \phi}{\partial y} = f (y - y_0) \tag{2}$$

where f is the focal length, and x and y are the displacements of the focal spots from the nominal position for a collimated beam, given by x_0 and y_0, respectively. The array of measured displacements of the focal spots can be integrated to reconstruct the wavefront.

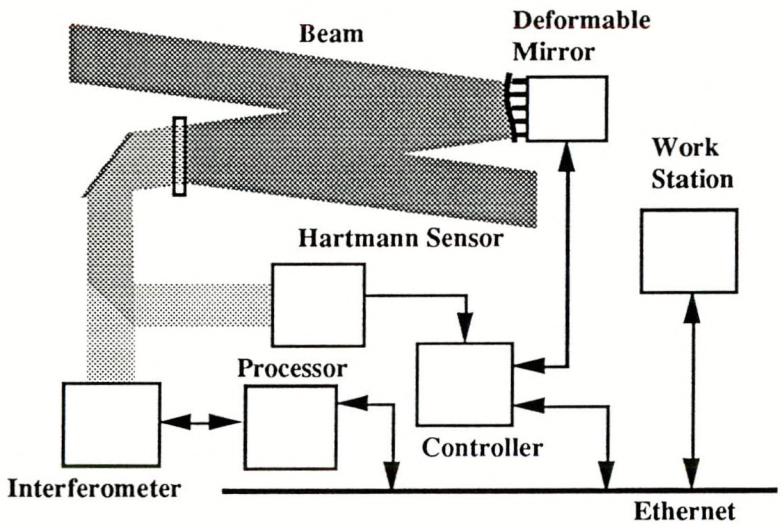

Fig. 1. Schematic of the AVLIS adaptive optics system. The ODC is the Processor—Optical Device Controller. The Hartmann sensor uses discrete lenses and position-sensitive photodiodes, and the deformable mirror is zonal actuated by PZTs. The controller uses a VME based architecture.

The appearance of dynamic spatial intensity modulation in the beam requires critical placement of the photodiodes in the focal plane of each lens. The modulation is caused partly by nonuniform pumping within the amplifiers. Spatial modulation is also caused by nonlinear interaction of beam diffraction within the channels of the amplifiers and saturation of the amplification when the amplifier is fully pumped. Since the output power from the dye chain is varied by changing the number of pump lasers and by turning off individual amplifiers (blocking the pump beams), both the magnitude and distribution of the spatial modulation are a function of power.

The effect of placing the photodiodes away from the focal plane under these conditions can be illustrated by a lens, which represents one channel of the Hartmann sensor. The procedure that we use to mount the photodiodes parallels this illustration. When the bottom half of the lens is blocked, the centroid of the transmitted light moves above the optical axis of the lens by 1/4 of the lens diameter. The centroid crosses the optical axis in the focal plane and moves below the optical axis after the focal plane. At the focal plane the centroid of the focus spot does not change when the half of the lens is

alternately blocked and unblocked. Since the displacement of the centroid is interpreted by the controller as an apparent local tilt, the apparent local tilt T (waves) can be related to the distance of the detector from the focal plane Δ by

$$T = \frac{\Delta \, D \, D_S}{4 \, f \, \lambda \, (f - \Delta)} \tag{3}$$

where D (5 mm) is the diameter of the lenslet, D_S (9.68 mm) is the spacing between lenslet axes, f (400 mm) is the focal length of the lenslet, and λ (600 nm) is the nominal wavelength. For this wavefront sensor, placing the detector within 0.3 mm of the focal plane of the lenslet results in an apparent wavefront tilt of less than 1/30th wave. Placing a chopper wheel in front of half the lens aperture and comparing the centroid of the half-blocked beam to that of the unblocked beam, we find dynamically the plane that minimizes the difference between the two measured centroids. This procedure minimizes the effect of changes in local spatial intensity modulation that occur during changes in amplification of the dye chain.

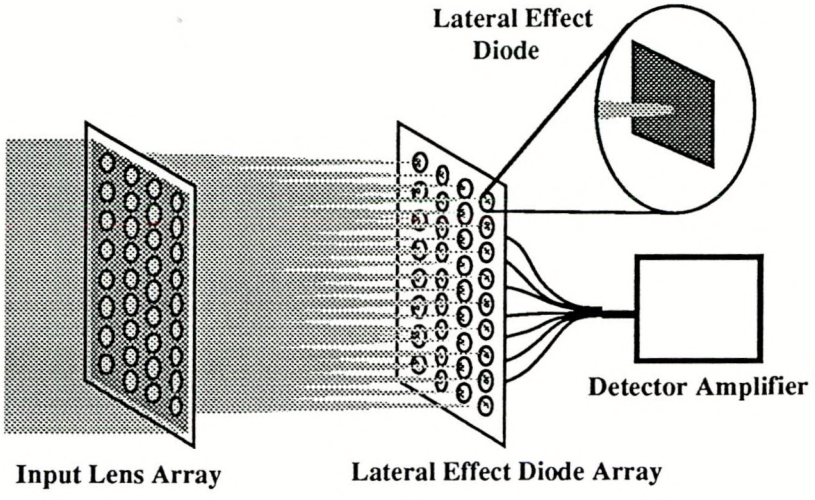

Fig. 2. Schematic of Hartmann sensor showing the discrete lenses and position-sensitive photodiodes. Photodiodes are mounted to within 0.3 mm of the focal plane; the nominal focal length of the *f* /80 lenses is 400 mm.

The four outputs from each photodiode are separated by an impedance of only 1KΩ. Furthermore, the dye light consists of 50 nsec pulses at a 4.3 kHz pulse rate. Chopper-stabilized transimpedance amplifiers are used as signal conditioners to isolate the outputs from each photodiode from the respective amplifier inputs. Conventional amplifiers exhibited significant zero-shift, and the positions of the measured centroids were very sensitive to the power of the incident beam. To minimize the ripple caused by the pulsed beam, the outputs of the amplifiers are filtered with an RC time constant of 300 msec. The measured centroids are unaffected by light level over a 20:1 range in intensity.

2.2 Deformable Mirror

The deformable mirror is a zonal design that consists of a 5x5 array of PZTs attached to the back of a monolithic glass substrate via flexures. Details of the design and testing of the deformable mirror are given in a companion paper by Swift et al.[3] A schematic showing the size and location of the attachment posts on the mirror is given in Fig. 3. Lenslet apertures of the Hartmann sensor, as well as the footprint of the beam, are superimposed on the mirror.

The mirror is designed to correct 2nd-order and 3rd-order aberrations of up to 5 waves p-v to within 1/10th wave rms across the beam; the mirror design also supports a closed-loop bandwidth of at least 1 Hz. The mirror is a dielectric coated, monolithic substrate of ULE that is 77 mm x 121 mm in size. To reduce stress-induced deformation of the front surface, both the front and back surfaces have a highly reflective dielectric coating. The substrate is thick enough to minimize ripples and bumps on the front surface from the actuators, which would impair the ability of the mirror to correct to the 1/10th wave

requirement. The substrate, however, is thin enough to have the required range in 3rd-order aberrations without breaking and without exceeding either the force or stiffness capabilities of available piezoelectric translators (PZTs).

The PZTs are obtained commercially and use integral strain gauges that compensate for both hysteresis and drift.[4] Feedback from the strain gauges increases the effective stiffness of the PZTs and, thus, minimizes the effect of changes in external loading by the substrate. The PZTs are attached to metal cups via flexures. The cups are bonded in shear to rectangular posts on the back of the substrate. The posts are formed by grinding the back surface of the mirror, followed by acid etching. The flexures minimize the lateral load by the mirror on the PZT without much loss in overall stiffness of the actuator assembly, and bonding to the mirror in shear minimizes stress-induced deformation of the mirror surface.

2.3 Controller Electronics

The 128 outputs from the Hartmann sensor must be measured with minimum time skew, especially in the presence of vibration, since changes in tilt during the sampling of the output channels would be interpreted as a higher order wavefront error. Hence, these outputs are latched simultaneously by sample-and-hold multiplexers and subsequently sent serially to an analog/digital converter. These electronics are located on a VME bus with a dedicated Motorola 68030 processor that monitors both the outputs from the Hartmann sensor and the PZT positions from the strain gauges on the deformable mirror and executes the wavefront correction algorithm. The signals from the controller are sent to a digital/analog converter; the analog signals are sent to custom PZT drivers that use analog strain-gauge feedback. The bandwidth of the analog strain-gauge feedback is 220 Hz.

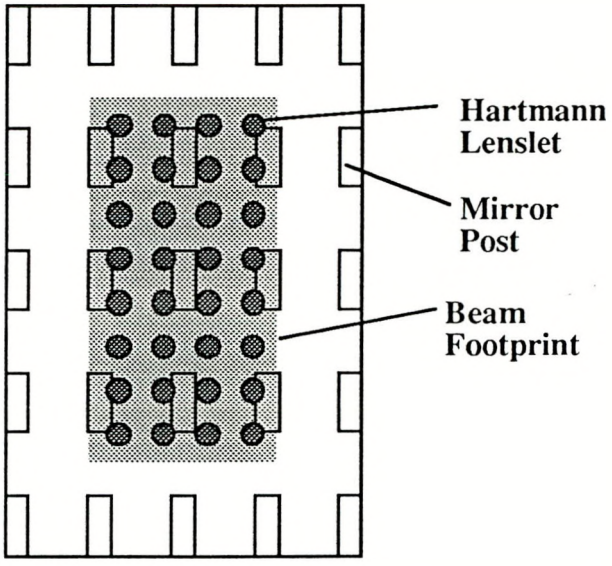

Fig. 3. Schematic of the deformable mirror showing the positions of the actuators, along with the footprint of the beam and the projection of the lenses of the Hartmann sensor. The mirror size is 77 mm x 121 mm.

2.4 Controller Algorithm

The presence of feedback from strain gauges on the PZTs enables us to directly control the displacement of the tip of the PZT instead of controlling the force exerted by the PZT. The following analysis will use indicial notation for matrix operations with implied summation over repeated indices.

The wavefront and the actuator command relationship can be described by Hooke's law,

$$k\, z_i = E_{ij}\, \phi_j \tag{4}$$

where z_i is the commanded displacement of the actuator, k is the stiffness of the actuator and flexure assembly, E_{ij} is the modulus of elasticity of the mirror at position j to a force ($k\ z_i$) exerted by an actuator at position i, and ϕ_j is the displacement of the mirror surface at position j. The displacement of the mirror surface can be replaced by the phase of the reflected wavefront, since the phase is related to the mirror surface by a factor of two.

If ϕ were a homogeneous function, then Euler's theorem for homogeneous functions of order n states that

$$x_j \left(\frac{\partial \phi}{\partial x}\right)_j + y_j \left(\frac{\partial \phi}{\partial y}\right)_j = n\ \phi_j \tag{5}$$

where the gradients $\partial\phi/\partial x$ and $\partial\phi/\partial y$ are measured by the Hartmann sensor at x_j and y_j, which are the coordinates of the sampling locations. In the case where ϕ is a surface of mixed order, Eq. (5) becomes an approximation. We can find a value C to replace the n in Eq. (5) that minimizes the difference between the two sides of the equation. Since the tilt of the wavefront is controlled separately by a pointing control mirror, the computation of C for a 3rd-order surface is generally aimed at seeking a compromise between the 2nd-order and the 3rd-order terms. The computation of C is imbedded in the minimization procedure described later in Eqs. (9)-(11). Equation (5) can be rewritten as

$$x_j \left(\frac{\partial \phi}{\partial x}\right)_j + y_j \left(\frac{\partial \phi}{\partial y}\right)_j = C\ \phi_j\ . \tag{6}$$

Substituting Eq. (6) into Eq. (4) for ϕ_j and letting k in Eq. (4) and C in Eq. (6) be absorbed in E, we obtain

$$z_i = E_{ij}\ r_{jk}\ s_k \tag{7a}$$

where

$$r_{jk} = x_j\ \delta_{jk} + y_j\ \delta_{j(k-m)} \tag{7b}$$

is the sampling location matrix (no implied summation over j),

$$s_k = \begin{cases} (\partial\phi/\partial x)_k & ;\quad 1 \le k \le m \\ (\partial\phi/\partial y)_{k-m} & ;\quad m+1 \le k \le 2m \end{cases} \tag{7c}$$

represents the slope measurements, and δ is the Kronecker Delta Function. Summation on k is from 1 to 2m, where m is the number of sampling locations of the Hartmann sensor. Note that r_{jk} is the concatenation of two diagonal matrices, each representing the respective x-locations and y-locations. Since the sampling locations are fixed, the only variables in Eq. (7a) are the slope values, and we can calculate the desired actuator displacements z_i from the measured slope values s_k. Replacing the sensor signal s by the difference between s and the set point s_0, we obtain from Eq. (7a)

$$z_i = G_{ik}\ (s_0 - s)_k \tag{8}$$

as the closed-loop feedback control law using the sensor signal directly as the controller input, where $G_{ik} = E_{ij}\ r_{jk}$.

2.5 Determination of the Gain Matrix

Previously, researchers such as Wallner[5] computed the control gain matrix **G** by minimizing the phase error. Measurement of phase requires a second instrument such as an interferometer to measure the same wavefront that the Hartmann sensor is measuring. An alternative is to integrate the slopes and fit the surface. The surface fitting requires a judicious choice of the fitting polynomial and may be computationally time consuming. Furthermore, the phase error obtained this way now contains the fitting error. The modulus of elasticity must be known explicitly to minimize the phase error.

We compute the gain matrix **G** by minimizing the actuator command error. Since the actuator command is related to the phase by a constant modulus of elasticity, as shown in Eq. (4) the two approaches are equivalent. The advantage of minimizing the actuator command error is that we are using information already available from the Hartmann sensor. Hence, we do not need phase information. Furthermore, minimizing the actuator error uses the modulus of elasticity implicitly.

The actuator error is minimized using the following analysis. The inner product of the residual actuator error summed over a set of measurements j is given by

$$\varepsilon_i = (z_{ij} - G_{ik}\, s_{kj})^2 . \tag{9}$$

The necessary condition for minimizing the inner product of the error is given by

$$\frac{\partial \varepsilon_i}{\partial G_{ik}} = -2\,(z_{ij} - G_{ik}\, s_{kj})\, s_{lj} = 0 \tag{10}$$

where l also refers to the Hartmann channel as does k. Solving for G_{ik} yields

$$G_{ik} = z_{ij}\, s_{lj}\, (\, s_{kj}\, s_{lj}\,)^{-1} . \tag{11}$$

Wallner used the same procedure except that he minimizes the phase error which is the difference between the phase (derived by surface fitting) and the predicted phase using **G** (which he calls **M**). He has also included the noise terms, while we have not. Most noise estimates used by other researchers only account for photon noise, while the noise in an operating facility also includes electronic noise, mechanical noise, turbulence and temperature variation. Although noise terms are helpful, they can not be obtained easily unless the operating conditions are constant. The laser transport system must operate under a wide range of power levels and dye flow rates, different wavelengths, and different combinations of amplifiers, to accommodate diverse test plans. An accurate estimate of the noise for one condition in a test run can not be uniformly applied to other runs. To offset the effect of noise, we add a gain scale factor in front of the gain matrix to maintain control stability under variable process conditions. This gain scale factor is determined from a conservatively determined signal-to-noise ratio.

3. SYSTEM PERFORMANCE TEST

The method that we used to verify the performance of the adaptive optics system was developed around two thoughts. First, the system performance must be verified interferometrically with an instrument that is independent of the control loop. Second, the system must be tested with input beams having up to five waves p-v of wavefront error, which forces the deformable mirror to operate far from the nominally flat condition. Any bumps or ripples induced by the actuators on the surface of the mirror during normal operation would be visible under this extreme condition.

3.1 Layout and Procedure

The layout of the system test is shown in Fig. 4 and is centered around a Wyko 6000 interferometer as the reference. The reference leg uses the beam from the interferometer, which is horizontally polarized. This beam is transmitted by the polarizer and reflected by the deformable mirror back to the interferometer. The control leg uses the output from a 35 mW HeNe laser, which is expanded, collimated, and transmitted through a 50/50 beam splitter. The transmitted beam, which is vertically polarized, is reflected by the polarizer and retroreflected by the deformable mirror. The reflected beam from the deformable mirror is directed back to the beam splitter, which reflects 50% into the Hartmann wavefront sensor. The polarizer is angle tuned to minimize the crosstalk between the reference leg and the control leg.

An aberrator that induces about 2.5 waves p-v of astigmatism on the transmitted beam was fabricated for testing our systems. In the test configuration shown in Fig. 4, the aberrator is double passed, resulting in about 5 waves of astigmatism as measured by both the interferometer and the Hartmann sensor when the mirror is flat. Insertion of the aberrator in front of the deformable mirror simulates an operating point at the design limit of the system.

The primary test is the following procedure. First, the deformable mirror is flattened manually using the Wyko interferometer with no aberrator in place. Once the mirror is flattened, the offsets of the focused spots on the diodes of the Hartmann sensor are recorded, which calibrates the Hartmann sensor to the flat wavefront. Then the controller is calibrated by measuring the influence function with the Hartmann sensor as each actuator is moved over a specified range. The gain matrix is obtained from this calibration as described above. At this point the system is calibrated. The system is then tested by inserting the aberrator in front of the deformable mirror and locking the control loop.

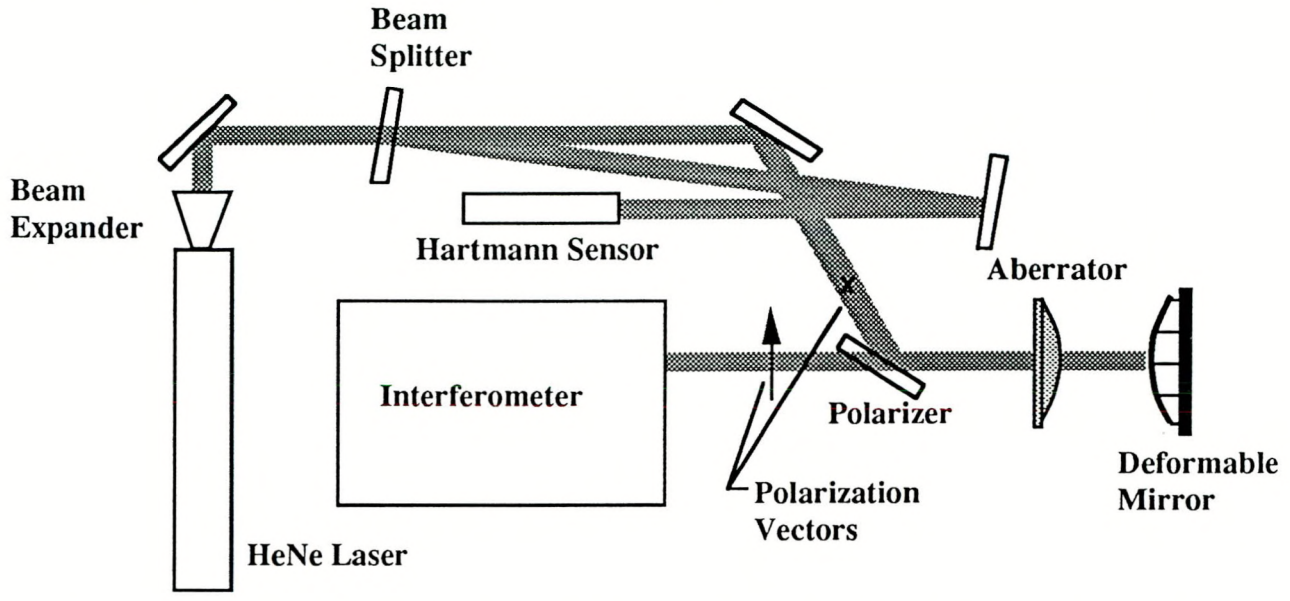

Fig. 4. Layout of test of system performance. The control leg is sensed by the Hartmann sensor, and the reference leg is sensed by the interferometer. The aberrator and the deformable mirror are in the common path for both legs.

Other tests of the controller include blocking the input to the Hartmann sensor while the control loop is locked. With no checking for intensity on the photodiodes the controller introduces random moves on the PZTs and, thus, wrinkles the mirror. The controller software limits the total difference in the displacement of adjacent actuators to 20 μm, which protects the mirror from accidental breakage. The Hartmann sensor is then unblocked, and the controller allowed to reflatten the reflected wavefront. When operated in the field, the controller only accepts data from the wavefront sensor when the intensity of the weakest channel exceeds a set threshold. This test was conducted both with the aberrator and without it.

3.2 Results

The results of the primary test are shown in Fig. 5, which shows contours of constant phase in the reflected wavefront from the aberrator-deformable mirror pair as a function of the number of iterations exercised by the controller. The contours are manually drawn traces from color contour plots from the interferometer; the contour levels in each plot are equally spaced and range from the peak to the valley of the wavefront. Also included are the p-v and rms of the reflected wavefront as measured by the interferometer. The plot for the aberrator was obtained with the mirror flat and immediately before the control loop was locked. By the sixth iteration the rms reflected phase is reduced by a factor of 10 to 0.11 waves. This residual phase error is after a correction of more than 5 waves p-v effective wavefront error on the beam incident on the deformable mirror. Little improvement was obtained after six iterations; however, Fig. 5 shows that the system reached 0.09 waves rms, which meets the 1/10th wave requirement. Since we have no rate information associated with the process, we assume a quasi-static process instead of a 2nd-order one. We used a scale factor for the gain matrix of 0.5. Hence, the loop should converge to within 98% of any fixed error in 6 iterations for noise-free data. The sampling rate for the wavefront sensor is about 7 Hz, which yields a closed-loop bandwidth of about 1 Hz.

The controller can return the mirror to a flat condition from any arbitrary initial condition, which was obtained by blocking the beam into the Hartmann sensor as described above. In these cases the residual reflected wavefront error is about 1/20th wave rms.

The time consumed by the controller in each iteration can be divided into [1] sampling the output from the Hartmann sensor and from the PZT strain gauges (28%), [2] matrix multiplication (14%), [3] comparing relative displacements between adjacent actuators and keeping them below a maximum value (30%), and [4] supporting calculations and sending control signals to the actuators through the digital/analog convertor (28%). Operation [1] has a total of 192 samples for each iteration. The supporting calculations include accounting for rotation of the lateral-effect diodes, subtraction of calibrated diode offsets for collimated light, and subtraction of diode setpoints for introducing preset curvature on the beam reflected by the deformable mirror. Operation [3] avoids the possibility of breaking the mirror by exceeding the tensile strength of the substrate. Future work will concentrate on reducing the computation time by optimizing the check of adjacent actuators and optimizing the supporting calculations by absorbing them into the matrix multiplication.

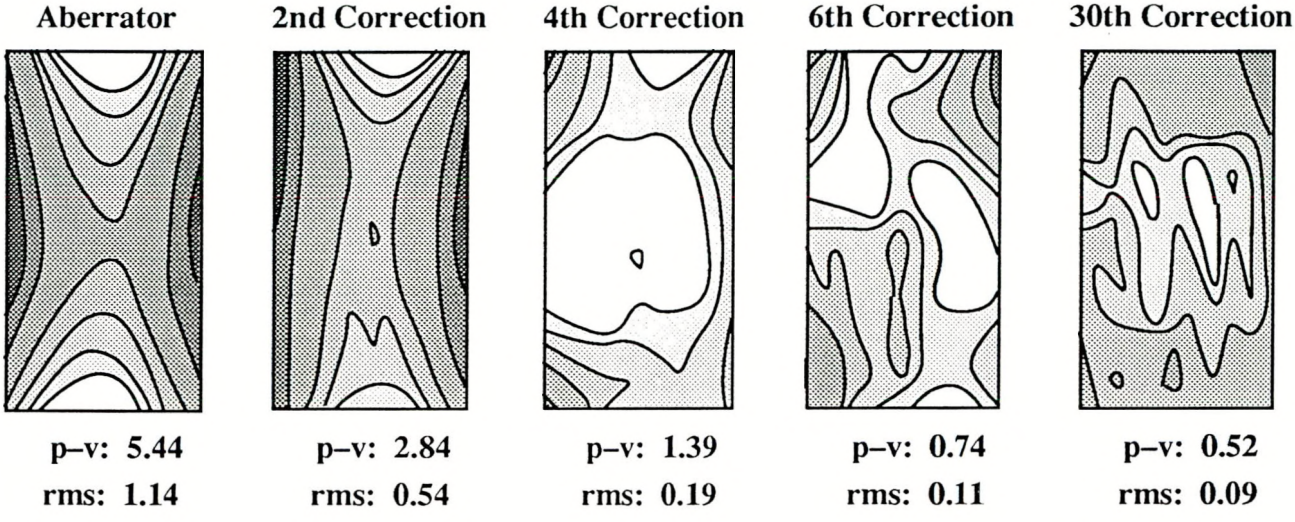

Fig. 5. Contour plots of the reflected wavefront from the aberrator and deformable mirror as measured by the interferometer for given iterations by the controller. The contours are equally spaced and cover the p-v range shown below each plot. The rms of the wavefront for each plot is also shown.

4. CONCLUSION

We have assembled and tested an adaptive optics system that uses a Hartmann sensor and a zonal deformable mirror. The residual error in the reflected wavefront is less than 1/10th wave rms over a range of ±5 waves p-v. The system is quasi-static and has a closed-loop bandwidth of 1 Hz, which is sufficient to correct thermally induced aberrations in transmissive optics. Future efforts will center on reducing the computation time taken by the controller.

5. ACKNOWLEDGEMENTS

Other contributors include Dick Thomas, who designed the signal conditioning electronics for the lateral effect diodes, Carolyn Weinzapfel, who conducted the interferometric measurements during the tests, and Marcus Libkind, who contributed to the design of the flexures on the back of the mirror.

6. REFERENCES

1. I. L. Bass, E. S. Bliss, R. E. Bonanno, P. Castle, M. Feldman, R. P. Hackel, P. R. Hammond, S. A. Johnson, R. Kichinski, K. Neeb, R. W. O'Neil, J. A. Paisner, R. P. Paris, and J. T. Salmon, "High Power performance of a copper laser pumped dye master-oscillator-power-amplifier chain," in *Technical Digest Conference for Lasers and Electro-Optics*, Optical Society of America, p. 392, 1991.

2. B. Platt and R. V. Shack, "Lenticular Hartmann Screen," *Optical Sciences Center Newsletter*, vol. 5, p. 15, March 1971.

3. C. D. Swift, J. W. Bergum, E. S. Bliss, F. A. House, M. A. Libkind, J. T. Salmon, and C. L. Weinzapfel, "Zonal Deformable Mirror for Laser Wavefront Control," SPIE Symposium on Optical Applied Science and Engineering, Paper No. 1543-10, San Diego, CA, July, 1991.

4. Manufactured by Physik Instrumente, Polytec Optronics, Inc., Costa Mesa, CA. 92626.

5. Edward P. Wallner, "Optimal wave-front correction using slope measurements," *J. Opt. Soc. Am.*, vol. 73, p. 1771-1776, 1983.